

OUTGASSING AS TRIGGER OF 1I/‘OUMUAMUA’S NONGRAVITATIONAL ACCELERATION: COULD THIS HYPOTHESIS WORK AT ALL?

ZDENEK SEKANINA

Jet Propulsion Laboratory, California Institute of Technology, 4800 Oak Grove Drive, Pasadena, CA 91109, U.S.A.

Version April 8, 2024

ABSTRACT

The question of what triggered the nongravitational acceleration of 1I/‘Oumuamua continues to attract researchers’ attention. The absence of any signs of activity notwithstanding, the prevailing notion is that the acceleration of the stellar, cigar-like object was prompted by outgassing. However, the Spitzer Space Telescope’s failure to detect ‘Oumuamua not only ruled out the CO₂ and/or CO driven activity (Trilling et al. 2018), but made the cigar shape incompatible with the optical observations. Choice of water ice as the source of outgassing is shown to be flawed as well: (i) the water sublimation law is demonstrably inconsistent with the observed variations in the nongravitational acceleration derived by Micheli et al. (2018), the point that should have been assertively highlighted; and (ii) an upper limit of the production rate of water is estimated at as low as 4×10^{23} molecules s⁻¹, requiring that, at most, only a small area of the surface be active. In this case the conservation of momentum law is satisfied only when ‘Oumuamua’s bulk density is extremely low, < 0.001 g cm⁻³, reminiscent of the formerly proposed scenario with ‘Oumuamua as a fragment of a dwarf interstellar comet, possibly an embryo planetesimal, disintegrating near perihelion, with the acceleration driven by solar radiation pressure (Sekanina 2019a) and no need for activity at all. High quality of astrometry and Micheli et al.’s orbital analysis, whose results were confirmed by the computations of other authors, is acknowledged.

Subject headings: interstellar objects: individual (1I/‘Oumuamua) — methods: data analysis

1. INTRODUCTION

Micheli et al.’s (2018) discovery of a nongravitational acceleration affecting the orbital motion of ‘Oumuamua continues to be attributed to outgassing, even though all efforts to detect a trace of activity failed. This situation prevails in part because a 3σ upper limit of the production rate of water, $Q_{\text{H}_2\text{O}} < 1.7 \times 10^{27}$ molecules s⁻¹, derived by Park et al. (2018) from their nondetection of the OH radio lines near 18 cm on 2017 November 12.97 UT (with the object 1.80 AU from the Sun), is rather soft. Ye et al. (2017) presented tighter 3σ upper limits on the production rates of three molecular species with emission bands at the optical wavelengths: $Q_{\text{CN}} < 2 \times 10^{22}$, $Q_{\text{C}_2} < 4 \times 10^{22}$, and $Q_{\text{C}_3} < 2 \times 10^{21}$ molecules s⁻¹, from their spectroscopic observations on October 26.21 UT, when the object’s heliocentric distance equaled 1.39 AU. Very important 3σ constraints were reported by Trilling et al. (2018) on the production rates of carbon dioxide, $Q_{\text{CO}_2} < 9 \times 10^{22}$ molecules s⁻¹, and of carbon monoxide, $Q_{\text{CO}} \lesssim 9 \times 10^{21}$ molecules s⁻¹, determined from their nondetection of ‘Oumuamua with the Spitzer Space Telescope during a set of exposures spanning nearly 33 hours and centered on November 22.11 UT, with the object then 2.00 ± 0.015 AU from the Sun. I show in Section 3 that all these limits can be used to provide independent constraints on the production of water.

2. RED FLAG IGNORED

The comprehensive study by Micheli et al. (2018) offers much insight into modeling the sublimation process and provides some useful constraints on the nature of the relevant mechanism by stating explicitly that: (i) the nongravitational effect is adequately described by a radial

acceleration only, with no need to incorporate the other two components; (ii) the introduction of discontinuities in the motion does not improve the data fit; and (iii) the variations with heliocentric distance r are consistent with r^{-2} or r^{-1} but not with any steeper laws, including the Style II model introduced by Marsden et al. (1973) to describe the nongravitational effects generated by the sublimation of water ice.¹ This result should have raised a **red flag**, as it amounts to a powerful **argument against the nongravitational acceleration in the orbital motion of ‘Oumuamua having been induced by the sublimation of water ice**. It is unfortunate that this major finding is noted by Micheli et al. only peripherally in the text and Table 1, but not explicitly in the executive summary.²

Micheli et al.’s nominal outgassing model requires — precisely for the reason just elaborated upon — a major contribution from carbon monoxide, whose sublimation rate varies, unlike that of water ice, as r^{-2} in the range of relevant heliocentric distances, thus complying with the observed law of variation. Since Trilling et al.’s (2018) results, based on the nondetection of ‘Oumuamua with the Spitzer Space Telescope, demonstrate conclusively that the nongravitational acceleration could under no circumstances be a corollary of the sublimation of carbon dioxide or carbon monoxide, I focus in this paper on providing a wealth of arguments to support the notion that the acceleration cannot in fact be a product of the sublimation of water ice either.

¹ Marsden et al.’s Style II model has successfully been employed to fit the orbital motions of a large number of comets in both short-period and nearly-parabolic orbits over the past nearly 50 years.

² Micheli et al.’s brief note on an improved model that is hugely asymmetric relative to perihelion is, as far as I noted, accompanied in their paper by no comment on the physical significance of ΔT , which I believe is in this case very probably none at all.

Table 1

3 σ Upper Limits of ‘Oumuamua’s Water Production Rate $Q_{\text{H}_2\text{O}}$ at 1.4 AU from the Sun Derived from CN, C₂, C₃ Limits by Ye et al. (2017) and CO, CO₂ Limits by Trilling et al. (2018), and from Ratios CN/OH, C₂/OH, C₃/OH, CO/H₂O, and CO₂/H₂O for Oort Cloud Objects

| Comet with Abundance Ratio(s) | Perihelion Distance (AU) | Reciprocal Semimajor Axis, ^a (1/a) _{orig} (AU ⁻¹) | Taxonomic Class Test ^b (C ₂ /CN) | ‘Oumuamua’s $Q_{\text{H}_2\text{O}}$ Upper Limit (10 ²⁵ s ⁻¹) ^c | | | | | Distance ^d from Sun (AU) | Abundance Ratio Reference |
|---------------------------------------|--------------------------|---|--|---|--------------------|--------------------|---------------------|-----------------------------------|-------------------------------------|----------------------------|
| | | | | CN/OH | C ₂ /OH | C ₃ /OH | CO/H ₂ O | CO ₂ /H ₂ O | | |
| C/1989 Q1 | 0.642 | -0.000218 ± 0.000022 | 1.38 | 0.49 | 0.71 | 0.85 | | | 1.18 A | A’Hearn et al. (1995) |
| C/1989 X1 | 0.350 | +0.000032 ± 0.000002 | 1.15 | 0.62 | 1.1 | 0.72 | | | 1.05 A | A’Hearn et al. (1995) |
| C/1999 S4 | 0.765 | +0.000003 ± 0.000002 | 0.60 | 1.9* | 6.9* | 3.2* | | | 1.06 B | Farnham et al. (2001) |
| | | | | 3.4* | 9.8* | 1.4* | | | 0.77 A | Farnham et al. (2001) |
| | | | | | | | 0.51 | | 0.83 B | Mumma et al. (2001) |
| C/2001 Q4 | 0.962 | +0.000028 ± 0.000001 | ? | | | | 0.04 | | 1.02 B | Lupu et al. (2007) |
| C/2007 N3 | 1.212 | +0.000022 ± 0.0000002 | 1.76 | 1.2 | 0.89 | 1.3 | | | 1.24 A | Bodewitz et al. (2011) |
| | | | | 0.96* | 2.0* | 0.27* | | | 2.61 B | Bair et al. (2018) |
| | | | | 1.1* | 1.4* | 0.30* | | | 1.77 A | Bair et al. (2018) |
| | | | | | | | | 0.80 ^e | 1.70 A | Ootsubo et al. (2010) |
| C/2012 S1 | 0.013 | +0.000035 ± 0.000006 | 1.95 | 2.1* | 2.2* | 0.61* | | | 1.67 B | Knight & Schleicher (2015) |
| Restricted Set ^f : typical | | | 1.15 | 0.63 | 1.1 | 0.78 | | | <3 BA | A’Hearn et al. (1995) |
| depleted | | | 0.25 | 1.0 | 8.0 | 3.0 | | | <3 BA | A’Hearn et al. (1995) |

Notes.

^a Referred to the barycenter of the Solar System; the values are from a variety of sources.

^b Averaged abundance ratio (C₂/CN); C₂/CN = 0.66 separates typical from carbon-chain depleted comets in A’Hearn et al.’s taxonomy.

^c Production rate’s upper limits from the five abundance ratios; values with asterisk are CN/H₂O, C₂/H₂O, and C₃/H₂O rates, respectively.

^d Average for a set of individual data points not too far apart; B = before perihelion, A = after perihelion.

^e Alternative result subsequently published by Ootsubo et al. (2012) implies an upper limit of $0.33 \times 10^{25} \text{ s}^{-1}$.

^f Selected set of 41 comets with at least three observations of five gaseous species (OH, CN, C₂, C₃, NH) made at less than 3 AU from the Sun.

3. CONSTRAINTS FROM GAS ABUNDANCE RATIOS

A meaningful upper limit of the water production rate for ‘Oumuamua can be estimated from the upper limits of the production rates of CN, C₂, C₃, CO, and CO₂, summarized in Section 1, combined with the known production rate ratios CN/OH, C₂/OH, C₃/OH (or directly CN/H₂O, C₂/H₂O, C₃/H₂O),³ CO/H₂O, and CO₂/H₂O for other appropriately chosen objects. Considering that ‘Oumuamua could have been part of an Oort Cloud of another stellar system (e.g., Do et al. 2018), the members of the Solar System’s Oort Cloud appear to be the closest analogs available for assessing ‘Oumuamua’s composition properties.

Table 1 lists six Oort Cloud comets used in this exercise. Columns 1–3, 5–9, and 11 are self-explanatory, while the fourth shows the test of A’Hearn et al.’s (1995) taxonomic class, (C₂/CN), an average of the ratio over the available data, identifying a member of the class of typical objects when it is ≥ 0.66 , or of the class of carbon-chain depleted objects otherwise. Of the six entries, only C/1999 S4 was carbon-chain depleted, while there are no data to classify C/2001 Q4. For comparison, I also include ‘Oumuamua’s water production rates derived from A’Hearn et al.’s average values for the groups of typical (70 percent of the total) and depleted objects in the restricted set, which contains the data obtained for the 41 comets that were well observed at heliocentric distances of less than 3 AU. The averages of the restricted set’s typical ratios amount to: CN/OH = 0.0032 ± 0.0013 , C₂/OH = 0.0036 ± 0.0017 , C₃/OH = 0.00026 ± 0.00017 ; for the depleted ones they are: CN/OH = 0.0020 ± 0.0007 ,

C₂/OH = 0.0005 ± 0.0004 , C₃/OH = 0.00007 ± 0.00004 . Column 10 specifies which part of the orbit do the data come from, listing an average heliocentric distance and the orbital branch, B if before or A if after perihelion.

The 3 σ upper limits of ‘Oumuamua’s production rate of water in Table 1 apply to a heliocentric distance of about 1.4 AU, at which Ye et al.’s (2017) observations were made and to which Micheli et al. (2018) refer their values as well. The production rates derived from the Spitzer Telescope observations (Trilling et al. 2018), were multiplied by a factor of four, implied by Marsden et al.’s (1973) Style II nongravitational law, to get converted to 1.4 AU. The results indicate that the H₂O upper limit is much tighter than $\sim 10^{27} \text{ molecules s}^{-1}$; five comets consistently show it to be more than two orders of magnitude lower, **3 to $6 \times 10^{24} \text{ molecules s}^{-1}$** , while the sixth comet, C/2001 Q4, offers a limit by yet another order of magnitude lower, **$4 \times 10^{23} \text{ molecules s}^{-1}$** . The data from the restricted set (A’Hearn et al. 1995), although of lesser relevance, suggest nearly equally low limits, including the class of carbon-chain depleted objects that generally provide somewhat higher, and less robust, limits.

In addition to the observationally established deficit of at least 3–4 orders of magnitude in the production rate of carbon monoxide (Trilling et al. 2018) and next to the contradiction in the nongravitational law (Section 2), **‘Oumuamua’s sublimation rate of water ice derived from five gas-abundance ratios is at least 1–2 orders of magnitude short of the production level required by the model interpreting the observed nongravitational acceleration as an outgassing-driven effect.** This major disparity increases to **at least 2–3 orders of magnitude for the pendulum-rotation model** proposed by Seligman et al. (2019).

³ The production rates of OH and H₂O are assumed equal, the other water dissociation and ionization products being neglected.

Table 2
Nongravitational Acceleration of Comet C/1998 P1 (Williams)

| | Nongravitational Parameter A_1 (10^{-8} AU day $^{-2}$) | Nongravi- tational Law ^a | Number of Obs. Used | Arc of Orbit Covered by Observations | Mean Residual | Computer |
|----------------------------|---|---|---------------------------|---|------------------|--------------|
| JPL Small-Body Database | 26.52 ± 0.30 | H ₂ O | 440 | 1998 Aug 11–1999 May 15 | $\pm 1''12$ | JPL SSD Team |
| MPC Orbits Database | 31.51 | H ₂ O | 372 | 1998 Aug 11–1999 Apr 14 | ± 0.7 | S. Nakano |
| S. Yoshida’s Comet Catalog | 31.44 ± 0.28 | H ₂ O | 398 | 1998 Aug 11–1999 May 15 | ± 0.76 | K. Muraoka |
| S. Nakano Notes (NK 1669) | 18.71 ± 0.15 | CO | 416 | 1998 Aug 11–1999 May 15 | ± 0.72 | S. Nakano |

Note.

^a H₂O = Marsden et al.’s (1973) Style II law for sublimation of water ice; CO = Yabushita’s (1996) law for sublimation of carbon monoxide ice.

4. COMPARISON WITH NONGRAVITATIONAL EFFECTS IN THE MOTIONS OF OTHER COMETS

Normalized to 1 AU from the Sun, the nongravitational acceleration detected by Micheli et al. (2018) in the orbital motion of ‘Oumuamua is 24.55×10^{-8} AU day $^{-2}$; it is directed radially away from the Sun and varies as an inverse second or first power of heliocentric distance.

To determine whether the magnitude of ‘Oumuamua’s nongravitational acceleration fares well in comparison with the outgassing-driven effects in the motions of long-period comets,⁴ I researched four online comet orbit catalogs: the *Jet Propulsion Laboratory’s* (JPL) Small-Body Database;⁵ the *Minor Planet Center’s* (MPC) Orbits/Observations Database;⁶ S. Yoshida’s cometary catalogue;⁷ and S. Nakano’s series of circulars.⁸ The net result of this extensive search was that the **number of objects** with a radial nongravitational acceleration comparable to, or greater than, ‘Oumuamua’s acceleration **was exactly one** — **C/1998 P1 (Williams)**, whose perihelion distance was 1.146 AU. However, as illustrated in Figure 1, the findings are complicated by the different nongravitational laws employed. From the orbit-determination details, listed in Table 2, it follows that the *integrated effect* of the nongravitational acceleration for C/1998 P1 was in fact smaller than for ‘Oumuamua. The parameter A_1 for C/1998 P1 slightly exceeded that for ‘Oumuamua only when the water ice sublimation law was forced through the observations (the JPL, MPC, and Yoshida entries in Table 2). When this law was replaced with Yabushita’s (1996) carbon-monoxide sublimation law (the Nakano Notes entry), which better fits the astrometric observations and closely matches the inverse square power law of heliocentric distance used by Micheli et al. (2018) for ‘Oumuamua, the parameter A_1 for C/1998 P1 dropped to merely $\frac{3}{4}$ ‘Oumuamua’s acceleration. The two objects also differed dramatically in their appearance, ‘Oumuamua looking stellar, the comet progressively more diffuse, displaying no nuclear condensation at all (DC = 0) when observed visually by Hale (2000) in March 1999, before disappearing on its way out. In any case, **‘Oumuamua’s orbital anomaly does**

not compare well with the outgassing-driven effects in the motions of long-period comets, exceeding even the largest among them by a sizable margin.

At the other extreme, the dwarf members of the Kreutz sungrazing system are subjected to much higher nongravitational accelerations than is ‘Oumuamua’s shortly before they sublimate away in the Sun’s corona (Sekanina & Kracht 2015), a scenario that is here irrelevant. Accelerations comparable to that of ‘Oumuamua are common among short-lived companions of the split comets, which are also of diffuse appearance and disintegrate on a time scale of weeks near 1 AU from the Sun (Sekanina 1982), also unlike ‘Oumuamua. In summary, there appears to be **no object whose outgassing-driven nongravitational effects and appearance both resemble ‘Oumuamua’s.**

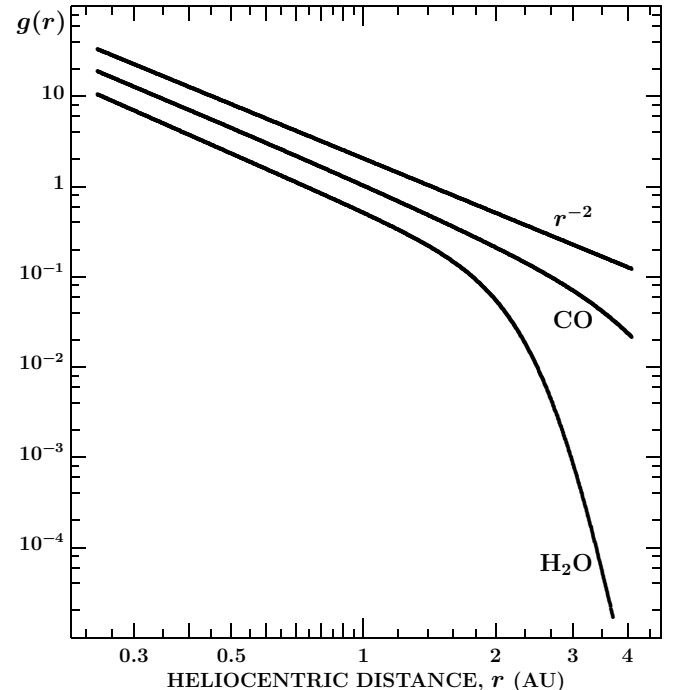


Figure 1. Comparison of three nongravitational laws $g(r)$. The H₂O curve is the standard Style II law by Marsden et al. (1973), describing the sublimation of water ice. The CO curve is the carbon monoxide law by Yabushita (1996), applied by Nakano to comet C/1998 P1. The r^{-2} curve is the inverse square power law of heliocentric distance employed by Micheli et al. (2018) for the nongravitational acceleration of ‘Oumuamua. The three curves are essentially equivalent up to about 1 AU from the Sun; the H₂O law then diverges rapidly. The curves are vertically shifted for clarity.

⁴ The radial component of the nongravitational acceleration has a different meaning for linked apparitions of the short-period comets, given the symmetric law employed (Sekanina 1993).

⁵ See https://ssd.jpl.nasa.gov/sbdb_query.cgi.

⁶ See https://minorplanetcenter.net/db_search; also the now-outdated printed catalogue by Marsden & Williams (2008).

⁷ See <http://www.aerith.net/comet/catalog/index-code.html>.

⁸ See <http://www.oaa.gr.jp/~oaaacs/nk.htm>.

5. WATER SUBLIMATION MODELING: THE INCONSISTENCIES

The next step in my pointing out the weaknesses of the interpretation of ‘Oumuamua’s nongravitational acceleration as a phenomenon driven by the sublimation of water ice is to demonstrate the implications, which are extreme. To start with, I consider a piece of matter of unit cross-sectional area, length ℓ , and uniform bulk density ρ , which includes at one end a layer of water ice sublimating at a constant rate of Z molecules per unit area per second with a speed v isotropically into a hemisphere whose boundary plane is perpendicular to the length ℓ , thus imparting to the rest of the body an acceleration Ψ . The conservation of momentum law dictates an equality

$$\rho\ell\Psi = \langle Zmv \rangle, \quad (1)$$

where m is the mass of a water molecule and $\langle Zmv \rangle$ is the component of the momentum change Zmv in the direction parallel to the body’s length, $\langle Zmv \rangle = \frac{2}{3}Zmv$; the components in all other directions cancel out.

Equation (1) represents the condition that the length ℓ of the body should, as a function of the bulk density, satisfy in order to fit the acceleration under the constraints. Given that ‘Oumuamua’s nongravitational acceleration varies as an inverse square of heliocentric distance, it equals $\Psi = 12.5 \times 10^{-8} \text{ AU day}^{-2} = 2.51 \times 10^{-4} \text{ cm s}^{-2}$ at 1.4 AU from the Sun. The standard equation of energy balance, applied to the solar flux incident on a Sun-facing planar surface of water ice, of an albedo of 0.1 and emissivity of 0.9, which is spent on the sublimation of the ice and on the black-body energy reradiation, provides at a heliocentric distance of 1.4 AU the sublimation rate of $Z = 6.9 \times 10^{17} \text{ molecules cm}^{-2} \text{ s}^{-1}$ and the temperature of $T = 199.8 \text{ K}$. In the absence of dust emission, the sublimation velocity equals, according to Probstein (1969), the speed of sound, $v_s = \sqrt{k_B \gamma_0 T / m}$, where k_B is the Boltzmann constant and γ_0 is the adiabatic index for water, amounting to 1.33. With the numerical values fitted in, $v_s = 3.50 \times 10^4 \text{ cm s}^{-1}$, yielding for the product of $\rho\ell$:

$$\rho\ell = 1920 \text{ g cm}^{-2}. \quad (2)$$

For $\rho \simeq 1 \text{ g cm}^{-3}$, for example, the length $\ell \simeq 20 \text{ m}$, a dimension significantly shorter than the expected characteristic size of ‘Oumuamua, in spite of the sublimation rate being maximized by assuming the normal incidence of the solar flux and neglecting the fraction of the solar energy that penetrates into the interior of the body. Equation (2) indicates that the length could be increased only by **lowering the bulk density**.

This elementary scenario is now expanded in two steps. First, in order to gain some insight, I assume a crude, spherical approximation, for which the nondetection of ‘Oumuamua by the Spitzer Space Telescope implies a diameter of less than 140 m at a visual geometric albedo of $p_V = 0.1$ or corresponding diameters at other albedo values according to Trilling et al. (2018). It should be remembered, however, that there are three conditions that need to be satisfied by a self-consistent solution simultaneously and that **the compliance** with all of them **still fails to remove the red-flag problem of the water sublimation law**, brought up to the reader’s attention in Section 2.

The first is the condition dictated by the conservation of momentum law, which now requires the determination of the contributions from all sublimating surface elements on the sunlit hemisphere to the component in the radial direction, that is, along the Sun-nucleus line. The sublimation rate at the subsolar point, Z_0 , is equal to the sublimation rate Z used above in the one-dimensional scenario. The sublimation rate $Z(\theta)$ at any other point on the sunlit hemisphere, at which the normal to the spherical surface makes an angle θ with the direction to the Sun, is lower because the incident solar flux amounts to only a $\cos \theta$ fraction of the solar flux at the subsolar point. I address this issue fully below in Section 6. For the purpose of the spherical approximation I assume that $Z(\theta) = Z_0 \cos \theta$ for any θ , which, as will be seen later, moderately exaggerates the actual sublimation rate. The sublimation velocity v_s decreases with increasing angle θ very slowly because of the nearly constant temperature, dropping at $\theta = 85^\circ$ to 0.94 the velocity at $\theta = 0^\circ$, an effect that is neglected in this first step. The sublimation rate from an annulus located between θ and $\theta + d\theta$ on the sunlit half of the spherical nucleus of diameter D equals $\frac{1}{2}\pi D^2 Z_0 \sin \theta \cos \theta d\theta$. A momentum per unit time transferred to the nucleus in the antisolar direction amounts to $\frac{1}{2}\pi D^2 (\frac{2}{3}Z_0 m v_s) \sin \theta \cos^2 \theta d\theta$. Summing up this expression over the sunlit hemisphere yields $\frac{1}{9}\pi D^2 Z_0 m v_s$ and the conservation of momentum law requires that

$$\frac{1}{6}\pi \rho D^3 \Psi = \frac{1}{9}\pi D^2 Z_0 m v_s, \quad (3)$$

where on the left is the product of the nucleus’ mass and acceleration. This expression simplifies to

$$\rho D \Psi = \frac{2}{3} Z_0 m v_s, \quad (4)$$

which is Equation (1) when $\ell = D$, $\langle Z \rangle = \frac{2}{3}Z_0$, and $v = v_s$.

The second condition is the requirement that the sublimation rate integrated over all surface elements be equal to the production rate $Q_{\text{H}_2\text{O}}$. Integrating, under the employed approximation, the sublimation rate from the annulus between θ and $\theta + d\theta$ over the entire sunlit hemisphere gives

$$Q_{\text{H}_2\text{O}} = \frac{1}{4}\pi D^2 Z_0. \quad (5)$$

The third condition equates the product of the projected area of the nucleus and the geometric albedo p_V with the intrinsic brightness:

$$\frac{1}{4}\pi D^2 p_V = X_0. \quad (6)$$

The quantities Ψ , Z_0 , v_s , and $Q_{\text{H}_2\text{O}}$ in the conditions (4) and (5) are heliocentric-distance dependent, while the condition (6) contains constants. In a previous paper (Sekanina 2019b) I remarked that, based on Drahus et al.’s (2018) data, the projected area of ‘Oumuamua at peak brightness equaled $0.002/p_V \text{ km}^2$. With the light-curve amplitude between 6:1 and 11:1, the mean projected area over a rotation cycle implies for the constant on the right-hand side of Equation (6) $X_0 = 0.0011 \text{ km}^2$. At $p_V = 0.1$, Equation (6) implies $D = 118 \text{ m}$, consistent with Trilling et al.’s (2018) upper limit of 140 m.

Continuing to refer the variable quantities to a heliocentric distance of 1.4 AU, I find from Equation (4)

$$\rho D = 1920 \text{ g cm}^{-2}, \quad (7)$$

which copies Equation (2), replacing only ℓ with D .

Adopting $\rho = 0.5 \text{ g cm}^{-3}$ as a typical bulk density of a cometary nucleus, this relation implies $D \simeq 38 \text{ m}$, a value about a factor of three smaller than derived above for $p_V = 0.1$ from Equation (6). Keeping the sublimation quantities in Equation (4) fixed at this point and avoiding unrealistically high albedos, this disparity can only be removed, as in Equation (2), by lowering the bulk density, in this case down to 0.16 g cm^{-3} . Next, by combining the conditions (4) through (6), I examine the constraints imposed by the water production rates established in Section 3 — the softer limit of $6 \times 10^{24} \text{ molecules s}^{-1}$ and the tighter limit of $4 \times 10^{23} \text{ molecules s}^{-1}$: (i) on Z_0 from an expression that is independent of D and ρ ; (ii) on D from an expression that is independent of ρ ; and (iii) on ρ from an expression that is independent of D .

The first constraint is obtained by eliminating πD^2 from Equations (5) and (6):

$$Z_0 = \frac{p_V Q_{\text{H}_2\text{O}}}{X_0}. \quad (8)$$

The second constraint is acquired directly from Equation (5):

$$D = \frac{2}{\sqrt{\pi}} \sqrt{\frac{Q_{\text{H}_2\text{O}}}{Z_0}}. \quad (9)$$

One can formulate two independent constraints on the bulk density. By eliminating D from (4) and (6) and then inserting for Z_0 from (8) one obtains

$$\rho = \frac{\sqrt{\pi} m v_s Q_{\text{H}_2\text{O}}}{3\Psi} \left(\frac{p_V}{X_0} \right)^{\frac{3}{2}}, \quad (10)$$

while by eliminating D from (4) and (5),

$$\rho = \frac{\sqrt{\pi} m v_s}{3\Psi} \sqrt{\frac{Z_0^3}{Q_{\text{H}_2\text{O}}}}. \quad (11)$$

The upper limit of $Q_{\text{H}_2\text{O}}$ offers, in Equation (8), an upper limit of Z_0 (to be compared with Z_0 from the equation of energy balance); in Equation (9), an upper limit of the nucleus’ diameter (to be compared with the photometric value of 118 m); and in Equation (10), an upper limit of the bulk density; besides, it provides, in Equation (11), a *lower* limit of the bulk density.

Inserting the numerical values, the problems emerge immediately; inserted into Equation (8), the two upper limits of the water production rate imply the sublimation rates of, respectively,

$$\begin{aligned} Z_0 &< 5.5 \times 10^{17} p_V = 0.55 \times 10^{17} \text{ molecules cm}^{-2} \text{ s}^{-1}; \text{ or} \\ Z_0 &< 0.36 \times 10^{17} p_V = 0.036 \times 10^{17} \text{ molecules cm}^{-2} \text{ s}^{-1} \end{aligned} \quad (12)$$

with the geometric albedo of $p_V = 0.1$; they are nowhere near the expected $Z_0 = 6.9 \times 10^{17} \text{ molecules cm}^{-2} \text{ s}^{-1}$. The constraint on the diameter of the object from (9) is likewise unacceptable

$$\begin{aligned} D &< 33 \text{ meters}; \text{ or} \\ D &< 8.6 \text{ meters}. \end{aligned} \quad (13)$$

The constraints on the bulk density are even more extreme; from Equation (10)

$$\begin{aligned} \rho &< 0.41 p_V^{\frac{3}{2}} = 0.013 \text{ g cm}^{-3}; \text{ or} \\ \rho &< 0.027 p_V^{\frac{3}{2}} = 0.00085 \text{ g cm}^{-3}, \end{aligned} \quad (14)$$

and from Equation (11)

$$\begin{aligned} \rho &> 0.58 \text{ g cm}^{-3}; \text{ or} \\ \rho &> 2.23 \text{ g cm}^{-3}. \end{aligned} \quad (15)$$

The upper limit of the bulk density is orders of magnitude below its lower limit, confirming that there is no way to make the nongravitational acceleration consistent with the upper limit of the water production rate under the given conditions.

The clue to removing the inconsistencies in modeling the production of water is by eliminating the discrepancy between the sublimation rates per unit area, Z_0 , determined from the energy balance equation on the one hand and by the inequalities (12) on the other hand. This effort is equivalent to making sure that the upper and lower limits of the bulk density equal each other, as both lines of attack lead to the crucial equation (8). To satisfy the tighter of the inequalities (12), the theoretical water sublimation rate per unit surface area of $Z_0 = 6.9 \times 10^{17} \text{ molecules cm}^{-2} \text{ s}^{-1}$ ought to be reduced by a factor of more than ~ 200 for $p_V \simeq 0.1$. This problem is solved by admitting that the **sublimation of water ice proceeds from less than 0.5 percent of the nucleus’ surface**. However, reducing Z_0 so dramatically has an effect on the condition in Equation (7), which now reads

$$\rho D < 9.6 \text{ g cm}^{-2}. \quad (16)$$

A diameter of 118 m then implies an **upper limit of only $\sim 0.0008 \text{ g cm}^{-3}$ for the bulk density of ‘Oumuamua**, thus making it an extremely porous object of exceptional, fluffy-like morphology, **a lookalike of the piece of debris of a dwarf interstellar comet, whose nongravitational acceleration was proposed to have been driven by solar radiation pressure** (Sekanina 2019a).

6. WATER SUBLIMATION MODELING REFINED

In step two of this exercise I remove the assumption of the spherical shape of ‘Oumuamua, which is contrary to observational evidence, and replace the approximate expressions for the water sublimation rate and temperature variations with the zenith distance of the Sun with more rigorous expressions, before addressing the three conditions represented in step one by Equations (4) to (6).

The shape of ‘Oumuamua is now approximated by a right circular cylinder, whose bases have a diameter of D and the side a length of ℓ . The object is either a disk ($D \gg \ell$), equivalent to an oblate-spheroid model; or a rod ($D \ll \ell$), equivalent to a prolate-spheroid model. In the existing terminology, ‘Oumuamua is being referred to as a pancake-shaped or cigar-shaped object, respectively. In the previous paper (Sekanina 2019b) I noted that only the pancake-like version was consistent with the non-detection by the Spitzer Telescope (Trilling et al. 2018), the cigar version’s dimensions exceeding the 3σ limits.

In order to verify or disprove the conclusions of the previous section, I deduce the expressions for the momentum change exerted on the object in the antisolar direction to replace Equation (4); for the overall water production from the object to replace Equation (5); and for its projected area to replace Equation (6); by averaging over all orientations of ‘Oumuamua relative to the Sun. For this purpose, the dependence of the water sublimation rate

Table 3

Relative Water Sublimation Rate $\zeta(\theta) = Z(\theta)/Z(0^\circ)$ and Sublimation Temperature at Heliocentric Distance of 1.4 AU As Function of Zenith Distance θ of the Sun^a

| Zenith Distance of Sun, θ | Sublim. Rate, ^b $\zeta(\theta)$ | Sublim. Temperature (K) | Zenith Distance of Sun, θ | Sublim. Rate, ^b $\zeta(\theta)$ | Sublim. Temperature (K) |
|----------------------------------|--|-------------------------|----------------------------------|--|-------------------------|
| 0° | 1.0000 | 199.81 | 45° | 0.6697 | 197.21 |
| 5 | 0.9956 | 199.78 | 50 | 0.5976 | 196.48 |
| 10 | 0.9829 | 199.69 | 55 | 0.5204 | 195.61 |
| 15 | 0.9614 | 199.55 | 60 | 0.4387 | 194.54 |
| 20 | 0.9318 | 199.34 | 65 | 0.3533 | 193.20 |
| 25 | 0.8939 | 199.07 | 70 | 0.2655 | 191.46 |
| 30 | 0.8486 | 198.73 | 75 | 0.1763 | 189.03 |
| 35 | 0.7956 | 198.32 | 80 | 0.0886 | 185.07 |
| 40 | 0.7359 | 197.81 | 85 | 0.0125 | 174.70 |

Notes.

^a Assumed: Bond Albedo = 0.1; Emissivity = 0.9.

^b Normalized to $Z(0^\circ) = 6.885 \times 10^{17}$ molecules $\text{cm}^{-2} \text{s}^{-1}$.

per unit surface area, $Z(\theta)$, and the sublimation temperature, $v_s(\theta)$, on the Sun's zenith distance θ have been computed by incorporating θ into the energy balance equation; for a heliocentric distance of 1.4 AU the results are presented in Table 3, in which $\zeta(\theta)$ is the relative sublimation rate per unit surface area at the Sun's zenith distance θ , expressed in units of the subsolar sublimation rate $Z(0^\circ)$, so that $Z(\theta) = Z(0^\circ) \cdot \zeta(\theta)$.

Because of the symmetry of the cylindrical model, only one of the two bases needs to be considered and only one half of the side. The position of the Sun is described by the angle θ its direction subtends with the axis of the cylinder, which is the Sun's zenith distance viewed from the base. The angle along the circumference of the base, ϕ , enters only a relation for the cylinder's side, measuring the angular distance from the plane passing through the Sun and the cylinder's axis. The sublimation rate at the subsolar point, $Z(0^\circ)$ in Table 3, is in the following abbreviated as Z_0 .

I now deal separately with either of the two parts of the momentum effect exerted by the water sublimation from the base and side of the cylindrical body. At an angle θ , the sublimation rate from a unit surface area of the base is $Z_0 \zeta(\theta)$, so that the contribution from this area to the momentum change in a direction normal to the surface is $\frac{2}{3} Z_0 \zeta(\theta) m v_s(\theta)$, where m is again the mass of a water molecule. This area's contribution to the momentum change in the antisolar direction is $\frac{2}{3} Z_0 \zeta(\theta) m v_s(\theta) \cos \theta$ and the overall contribution from the base at the Sun's zenith distance θ is

$$\frac{1}{4} \pi D^2 \cdot \frac{2}{3} Z_0 \zeta(\theta) m v_s(\theta) \cos \theta. \quad (17)$$

The Sun's position, described by a zenith distance θ as viewed from the base of the cylinder, makes a minimum angle of $90^\circ - \theta$ with the surface of its side along the stripe extending in the plane that contains the Sun and the cylinder's axis. At all other points of the cylinder's sunlit side the Sun's zenith distance is in the range between $90^\circ - \theta$ and 90° . The side's peak sublimation rate from a unit surface area is therefore $Z_0 \zeta(90^\circ - \theta)$ and its contribution to the momentum change in the antisolar direction equals $\frac{2}{3} Z_0 \zeta(90^\circ - \theta) m v_s(90^\circ - \theta) \sin \theta$. A stripe

of an infinitesimal width of $\frac{1}{2} D d\phi$ and the length ℓ between both bases contributes

$$\frac{1}{2} D \ell d\phi \cdot \frac{2}{3} Z_0 \zeta(90^\circ - \theta) m v_s(90^\circ - \theta) \sin \theta. \quad (18)$$

A similar stripe of infinitesimal width whose normal to the surface of the side subtends with the Sun an angle ψ and with the plane passing through the Sun and the cylindrical axis an angle ϕ reckoned in this plane in both directions along the circumference of the base, sublimates at the Sun's zenith angle of $90^\circ - \theta$ at a rate of $Z_0 \zeta(\psi)$, where the angle ψ depends on θ and ϕ through a relation

$$\cos \psi = \sin \theta \cos \phi. \quad (19)$$

This stripe's contribution to the momentum change in the antisolar direction is

$$\frac{1}{2} D \ell d\phi \cdot \frac{2}{3} Z_0 \zeta(\psi) m v_s(\psi) \cos \psi. \quad (20)$$

It is noted that $\psi = 90^\circ - \theta$ and the expression (20) becomes identical with (18) when $\phi = 0^\circ$. Integrating the contributions to the momentum change in the antisolar direction over the surface of the sunlit half of the cylindrical side, I find for the Sun's angle θ ,

$$\begin{aligned} & \frac{1}{3} D \ell Z_0 m \int_{-\frac{\pi}{2}}^{\frac{\pi}{2}} \zeta(\psi) v_s(\psi) \cos \psi d\phi \\ \text{or} \\ & \frac{2}{3} D \ell Z_0 m \int_{\frac{\pi}{2}-\theta}^{\frac{\pi}{2}} \frac{\zeta(\psi) v_s(\psi) \sin \psi \cos \psi}{\sqrt{\sin^2 \theta - \cos^2 \psi}} d\psi \\ \text{or} \\ & \frac{2}{3} D \ell Z_0 m \sin \theta \int_0^{\frac{\pi}{2}} \zeta(\psi) v_s(\psi) \cos \phi d\phi. \end{aligned} \quad (21)$$

In summary, the momentum change $\dot{\mu}(\theta)$, exerted on 'Oumuamua in the antisolar direction at the Sun's angle θ is given by adding the expressions (17) and (21),

$$\begin{aligned} \dot{\mu}(\theta) = & \frac{1}{6} D Z_0 m \left[\pi D \zeta(\theta) v_s(\theta) \cos \theta \right. \\ & \left. + 4 \ell \sin \theta \int_0^{\frac{\pi}{2}} \zeta(\psi) v_s(\psi) \cos \phi d\phi \right]. \end{aligned} \quad (22)$$

Averaging over all angles θ , the mean momentum change in the antisolar direction, $\langle \dot{\mu} \rangle$, becomes

$$\begin{aligned} \langle \dot{\mu} \rangle = & \int_0^{\frac{\pi}{2}} \dot{\mu}(\theta) \sin \theta d\theta \\ = & \frac{1}{6} D Z_0 m \int_0^{\frac{\pi}{2}} \left[\pi D \zeta(\theta) v_s(\theta) \cos \theta \right. \\ & \left. + 4 \ell \sin \theta \int_0^{\frac{\pi}{2}} \zeta(\psi) v_s(\psi) \cos \phi d\phi \right] \sin \theta d\theta, \end{aligned} \quad (23)$$

where the angle ψ is computed from Equation (19). The conservation of momentum condition now requires that

$$\langle \dot{\mu} \rangle = \frac{1}{4} \pi \rho D^2 \ell \Psi, \quad (24)$$

where Ψ is, as before, 'Oumuamua's nongravitational acceleration.

The expression for 'Oumuamua's production rate of water is derived in a manner similar to the expression

for the momentum change. For any particular direction θ I find for the production rate summed up from the sunlit base and side,

$$Q_{\text{H}_2\text{O}}(\theta) = \frac{1}{4}\pi D^2 Z_0 \zeta(\theta) + 2D\ell Z_0 \int_0^{\frac{\pi}{2}} \zeta(\psi) d\phi, \quad (25)$$

where ψ is again given by Equation (19). Averaging over all angles θ gives for the water production rate

$$\langle Q_{\text{H}_2\text{O}} \rangle = \frac{1}{4}DZ_0 \int_0^{\frac{\pi}{2}} \left[\pi D \zeta(\theta) + 8\ell \int_0^{\frac{\pi}{2}} \zeta(\psi) d\phi \right] \sin \theta d\theta. \quad (26)$$

Viewed from a direction θ , the sunlit projected area of ‘Oumuamua equals in the cylinder approximation

$$X(\theta) = \frac{1}{4}\pi D^2 \cos \theta + D\ell \sin \theta, \quad (27)$$

which, when averaged over a hemisphere, becomes

$$\langle X \rangle = \frac{1}{4}\pi D \left(\frac{1}{2}D + \ell \right). \quad (28)$$

Expression (27) implies the presence of two minima and two maxima per rotation. The minima take place at $\theta = 0^\circ$ and $\theta = 90^\circ$, the shallower one bounded by the maxima satisfying a condition $\tan \theta = 4\ell/\pi D$, implied by Equation (27). When the cylinder is a disk ($D \gg \ell$), the shallow minimum is at $\theta = 0^\circ$ and the deep at $\theta = 90^\circ$; when a rod ($D \ll \ell$), it is the other way around. For a disk, the peak projected area is given by

$$X_{\text{max}} = \frac{1}{4}\pi D^2 \sqrt{1 + \left(\frac{4\ell}{\pi D} \right)^2}. \quad (29)$$

Since the projected area at the deep minimum now equals $X_{\text{min}} = D\ell$, the ratio $X_{\text{max}}/X_{\text{min}} = \mathcal{A}$, determining the amplitude of the light curve, is

$$\mathcal{A} = \sqrt{1 + \chi^2}, \quad (30)$$

where $\chi = \pi D/4\ell$. When the cylinder is a rod, it is more convenient to write

$$X_{\text{max}} = D\ell \sqrt{1 + \left(\frac{\pi D}{4\ell} \right)^2}. \quad (31)$$

As the projected area at the deep minimum in this case equals $X_{\text{min}} = \frac{1}{4}\pi D^2$, the ratio \mathcal{A} is again given by Equation (30), in which though now $\chi = 4\ell/\pi D$, a reciprocal of the expression for the disk.

The amplitudes of the shallow minima are also given by Equation (30), but with the expressions for χ interchanged: $\chi = 4\ell/\pi D$ for a disk, but $\chi = \pi D/4\ell$ for a rod.

An interesting byproduct of the disk vs rod scenarios is that for the same peak projected area, X_{max} , and the same amplitude, \mathcal{A} — and therefore also for the same minimum projected area, X_{min} — the volume of the disk is always significantly smaller than the volume of the rod, by a factor of $(\mathcal{A}^2 - 1)^{\frac{1}{4}}$, which amounts, for example, to 2.43 for $\mathcal{A} = 6:1$ used below; the volume equals

$$\mathcal{V} = \frac{\sqrt{\pi}}{2} \left(\frac{X_{\text{max}}}{\mathcal{A}} \right)^{\frac{3}{2}} (\mathcal{A}^2 - 1)^\kappa, \quad (32)$$

where κ equals $\frac{1}{4}$ for the disk but $\frac{1}{2}$ for the rod.

Numerically, a light-curve amplitude \mathcal{A} of 6:1 implies $D/\ell = 7.5$ for a disk and $\ell/D = 4.6$ for a rod. Similarly, an amplitude of 11:1 is equivalent to $D/\ell = 13.9$ for a disk and $\ell/D = 8.6$ for a rod. The reciprocal ratios indicate extremely small amplitudes for the shallow minima, not exceeding 0.02 mag, thus effectively retracting the above statement about two minima and two maxima — the projected area at, and in between, these maxima is essentially constant.

Recalling once again ‘Oumuamua’s peak projected area of $X_{\text{max}} = 0.02 \text{ km}^2$ at $p_V = 0.1$ (Sekanina 2019b), based on Drahus et al.’s (2018) photometric observations, I now used Equations (29) through (31) to determine the dimensions of the object’s cylindrical (both disk and rod) model. In order that the results could directly be compared with the 3σ upper limit determined by Trilling et al. (2018), for the same assumed value of the albedo p_V , from the nondetection of ‘Oumuamua by the Spitzer Space Telescope, I adopted $\mathcal{A} = 6:1$. For the **disk** version I obtained $D = 158 \text{ m}$, $\ell = 21 \text{ m}$, both deep **within Trilling et al.’s limits** of 341 m by 57 m, but for the rod version I got $\ell = 303 \text{ m}$, $D = 65 \text{ m}$, the **rod’s diameter failing to fit the limit**. This outcome demonstrates that the **only plausible solution is the disk**, paralleling the result of a pancake vs cigar comparison examined in Section 9 of Sekanina (2019b).

In order to facilitate the integration of the expressions for the momentum change and the production rate, I fit $\zeta(\theta)$ and $T(\theta)$ [needed to determine $v_s(\theta)$], the two quantities given in tabular form, by explicit functions. For the dependence of the relative sublimation rate of water ice per unit surface area on the Sun’s zenith distance I find a good approximation to be

$$\zeta(\theta) = \cos \theta - 0.068 \theta^{2.1} \left(\frac{1}{2}\pi - \theta \right)^{0.8}, \quad (33)$$

where θ is in radians; and similarly, for the sublimation temperature (in K),

$$T(\theta) = 199.81 - 3.55 \theta^{1.8} (1.58 - \theta)^{-0.5}. \quad (34)$$

The first terms on the right-hand side represent in both expressions the crude approximations, with the correction terms following. It is noted that the first terms were employed to approximate $\zeta(\theta)$ and $T(\theta)$ in Section 5. The constant 1.58 in Equation (34) is used instead of $\frac{1}{2}\pi$ to avoid the negative, indeterminate value of T at $\theta = 90^\circ$. The computed sublimation temperatures near this limit are immaterial, because the relevant areas of the surface provide only a minute contribution to the total momentum change.

This completes the steps necessary to integrate Equations (23) and (26) and thus to examine the refined sublimation model. The results of the computations are summarized in Table 4 for both the viable, disk-like scenario and the rejected, rod-like scenario, which contradicts the Spitzer Space Telescope’s nondetection of ‘Oumuamua. The results generally confirm the findings based on the approximate method used in Section 5, even though the bulk density constraint is now slightly less unfavorable to the hypothesis of outgassing-driven nongravitational acceleration: the tighter constraint on the water production rate in Section 3 implies that a **3σ upper limit on ‘Oumuamua’s bulk density in the disk case amounts to 0.0015 g cm^{-3}** and is still lower in the rod case.

Table 4

Averaged Momenta Changes and Production Rates of Water for the Disk- and Rod-Shaped Models of 1I/‘Oumuamua Under Condition of Equal Projected-Area Range for Maximum-to-Minimum Ratio of 6:1 at Heliocentric Distance of 1.4 AU

| Quantity | Disk Shaped | Rod Shaped |
|--|-------------|------------|
| Maximum projected area, X_{\max} (km ²) | 0.020 | 0.020 |
| Minimum projected area, X_{\min} (km ²) | 0.0033 | 0.0033 |
| Averaged projected area, $\langle X \rangle$ (km ²) | 0.0124 | 0.0171 |
| Diameter of base, D (m) | 158 | 65 |
| Length of side, ℓ (m) | 21 | 303 |
| Volume, V (10 ⁶ m ³) | 0.41 | 1.01 |
| Surface completely ice covered: | | |
| Averaged momentum change in antisolar direction, $\langle \dot{\mu} \rangle$ (10 ⁶ g cm s ⁻²) | 38 | 52 |
| Averaged production rate, $\langle Q_{\text{H}_2\text{O}} \rangle$ (10 ²⁵ s ⁻¹) | 10 | 21 |
| Bulk density, ρ , to satisfy Eq. (24) (g cm ⁻³) | 0.36 | 0.50 |
| Constraint ^a by $Q_{\text{H}_2\text{O}} < 0.6 \times 10^{25} \text{ s}^{-1}$: | | |
| Fraction of ice-covered surface (percent) | <6.0 | <2.9 |
| Bulk density, ρ , to satisfy Eq. (24) (g cm ⁻³) | <0.022 | <0.014 |
| Constraint ^a by $Q_{\text{H}_2\text{O}} < 0.04 \times 10^{25} \text{ s}^{-1}$: | | |
| Fraction of ice-covered surface (percent) | <0.40 | <0.19 |
| Bulk density, ρ , to satisfy Eq. (24) (g cm ⁻³) | <0.0015 | <0.0010 |

Note.

^a See Section 3 and Table 1.

7. DISCUSSION

It has to be remembered that the derived constraints, as 3σ upper limits, exceed in all probability the actual values of the water production rate and the sublimation-driven momentum change by orders of magnitude, or that the two are simply zero. The bulk density should also be substantially lower, so that — significantly — the examination of this hypothesis leads to the same conclusion as the model in which the nongravitational acceleration is driven by solar radiation pressure and which requires the object’s extremely high porosity and degree of fluffiness. Such a model was advocated in my previous paper based on the argument that ‘Oumuamua was a piece of inactive debris of a disintegrated dwarf interstellar comet (Sekanina 2019a).

I already pointed out in Section 5 that the issue of water abundance is separate from the *red-flag* problem of the incorrect law of variation with heliocentric distance that the sublimation of water ice offers to fit the nongravitational acceleration. Another problem, a dramatically different appearance of ‘Oumuamua and comets with similarly high nongravitational accelerations, was commented on in Section 4.

The red-flag problem of the sublimation law is important enough that it should be examined in the framework of the cylindrical model for ‘Oumuamua. In Section 6 and Tables 3 and 4 I listed the information that this model provided for the heliocentric distance of 1.4 AU, at which the upper limits of the production rates of CN, C₂, and C₃ were obtained by Ye et al. (2017) and to which the upper limits of CO₂ and CO by Trilling et al. (2018) could be converted with sufficient accuracy. Since ‘Oumuamua was discovered only about a week earlier, the heliocentric distance of 1.4 AU characterizes the pe-

Table 5

Relative Water Sublimation Rate $\zeta(\theta) = Z(\theta)/Z(0^\circ)$ and Sublimation Temperature at Heliocentric Distance $r = 2.9$ AU As Function of Zenith Distance θ of the Sun^a and Comparison With $r = 1.4$ AU (Table 3)

| Zenith Distance of Sun, θ | Relative Sublimation Rate ^b of Water, $\zeta(\theta)$ | Sublimation Temperature, T (K) | Comparison with 1.4 AU | |
|----------------------------------|--|----------------------------------|--------------------------------------|-------------------------------------|
| | | | Average Value of n in Law r^{-n} | Drop in Temperature, ΔT (K) |
| 0° | 1.0000 | 188.06 | 2.61 | 11.75 |
| 10 | 0.9752 | 187.91 | 2.62 | 11.78 |
| 20 | 0.9022 | 187.46 | 2.66 | 11.88 |
| 30 | 0.7838 | 186.65 | 2.72 | 12.08 |
| 40 | 0.6260 | 185.38 | 2.83 | 12.43 |
| 50 | 0.4374 | 183.38 | 3.04 | 13.10 |
| 60 | 0.2340 | 179.99 | 3.48 | 14.55 |
| 70 | 0.0548 | 172.59 | 4.78 | 18.87 |
| 80 | 0.0002 | 149.17 | 10.90 | 35.90 |

Notes.

^a Assumed: Bond Albedo = 0.1; Emissivity = 0.9.

^b Normalized to $Z(0^\circ) = 1.028 \times 10^{17} \text{ molecules cm}^{-2} \text{ s}^{-1}$.

riod of time when the object was at its brightest. In order to appreciate the presumed activity changes over nearly the entire orbital arc over which ‘Oumuamua was under observation, I list in Table 5 the sublimation data, arranged similarly to Table 3, for a heliocentric distance of 2.9 AU that corresponds to the last observations with the Hubble Space Telescope in early January 2018. The last two columns allow comparison of the expected decrease in both the sublimation rate and temperature over the period of more than two months that the range of heliocentric distances from 1.4 to 2.9 AU represents. The issue of the sublimation law is addressed in column 4, which shows the inverse power n of heliocentric distance r , with which the sublimation rate is expected to drop between 1.4 and 2.9 AU as a function of the Sun’s zenith distance θ . At the subsolar point the rate varies as $r^{-2.6}$, but it becomes progressively steeper with increasing θ , reaching r^{-3} at 50° and nearly r^{-5} at 70°, in contrast with the rate of r^{-1} to r^{-2} established by Micheli et al. (2018). The last column of Table 5 shows that the sublimation temperature dropped by about 12 K between 1.4 and 1.9 AU near the subsolar point but much more at large zenith distances.

In order to examine the integrated effect of the distribution of the sublimation rate and temperature over the cylindrical model of ‘Oumuamua, I now applied the procedure developed in Section 6 to the heliocentric distance of 2.9 AU. It was necessary to replace the expressions (33) for $\zeta(\theta)$ and (34) for $T(\theta)$ with new ones; it turned out that their general form was applicable, with only most of the constants having different values. The integration showed that for the surface completely covered with water ice the averaged momentum changes $\langle \dot{\mu} \rangle$ and production rates $\langle Q_{\text{H}_2\text{O}} \rangle$ equaled at 2.9 AU from the Sun:

$$\begin{aligned}
 \langle \dot{\mu} \rangle &= 4.4 \times 10^6 \text{ g cm s}^{-2} && \text{for disk,} \\
 &= 6.1 \times 10^6 \text{ g cm s}^{-2} && \text{for rod,} \\
 \langle Q_{\text{H}_2\text{O}} \rangle &= 0.94 \times 10^{25} \text{ molecules s}^{-1} && \text{for disk,} \\
 &= 2.03 \times 10^{25} \text{ molecules s}^{-1} && \text{for rod.} \quad (35)
 \end{aligned}$$

Combining these numbers with the relevant data from Table 4, I find that, **regardless of the level of activity or the lack of it**, the momentum effect driven by the sublimation of water ice should vary as $r^{-3.0}$ and the production rate as $r^{-3.2}$. As explicitly remarked by Micheli et al. (2018), **this rate of variation is “strongly disfavored by the data”**.

Although the present scenario is different from Micheli et al.’s (2018) model, the predicted total *mass* production rates at 1.4 AU from the Sun agree to within 20 percent of each other: I find 3.0 kg s^{-1} (for the disk case), whereas Micheli et al. get 3.6 kg s^{-1} when the contributions from water ice and carbon monoxide are added up. Both models are comparable in their flexibility to accommodate the observational constraints in terms of the upper limits of the bulk density and the fraction of the surface that is active. On the other hand, because of the “ray tracing” of migrating activity over the surface, the rigidity of Seligman et al.’s (2019) model does not allow the option of relegating outgassing to a tiny fraction of the surface and their model, requiring a water production rate as high as 9 kg s^{-1} ($3 \times 10^{26} \text{ molecules s}^{-1}$), is out of line with the production-rate constraints, as already noted briefly in Section 3. These authors do not address the problem with the sublimation law and there are other problems with their model, the two most worrisome being: (i) the derived dimensions of the object’s model violate, contrary to their claim, the constraints set by the nondetection of ‘Oumuamua by the Spitzer Space Telescope (Trilling et al. 2018);⁹ and (ii) the carbon-to-oxygen ratio obtained from their water production rate and Trilling et al.’s upper limits on the production rates of carbon dioxide and carbon monoxide reaches an extremely low upper limit of $\text{C/O} < 0.0003$, the authors’ value of 0.003 resulting from their two-orders-of-magnitude error in quoting Trilling et al.’s constraint on the production of CO.¹⁰ Among the 18 comets with the H_2O , CO_2 , and CO production rates tabulated by Ootsubo et al. (2012), the lowest C/O ratio is ~ 0.04 , and with a few exceptions CO_2 is more abundant than CO, in line with Trilling et al.’s numbers; for the only Oort Cloud comet on Ootsubo et al.’s list, C/2007 N3 (Lulin), the C/O ratio is between 0.08 and 0.10 and CO_2/CO ratio is > 5 . Comets with extremely low ratios of C/O, of < 0.001 , if they exist at all, must be exceptionally rare: Ootsubo et al. do not have any on their list, Reach et al. (2013) do very few, all highly uncertain and therefore dubious.

The problem of the nongravitational law actually illustrates a high quality of both the astrometric observations employed by Micheli et al. (2018) and their orbital analysis. I note with surprise a recent paper by Katz (2019), who questions Micheli et al.’s results. His objections are of two types, physical and methodical. While I understand his uneasiness about an implied dust-to-gas ratio of < 0.0005 , I see **no substantiation** for a conclusion that **‘Oumuamua’s orbital motion was affected by no (or**

nearly no) force other than the Sun’s gravity. While my impression is that the presence of a nongravitational acceleration was unequivocally and convincingly demonstrated by Micheli et al., Katz’s doubts should be confronted with independent evidence. Since the set of more than 200 astrometric positions was supplied by nearly 30 groups of observers, it is only the method of orbital analysis, which, if overreaching, could make a difference. In the following, Micheli et al.’s findings are compared with the orbit determinations by other authors.

Nakano (2018) used his own computer code to investigate ‘Oumuamua’s orbital motion, tabulating individual residuals (listed unfortunately only to the nearest $0''.1$) from two orbital solutions: a gravitational one and Marsden et al.’s (1973) Style II nongravitational one, solving for the radial and transverse components of the acceleration. The residuals are quite small, with the mean residual of $\pm 0''.42$ for the gravitational solution and $\pm 0''.33$ for the nongravitational solution. A greater difference between both solutions is in the *systematic trends* displayed by the residuals, which are most consistent and therefore best seen among the positions derived from images taken with the Hubble Space Telescope (HST) on 2017 November 21–22 (15 data points), December 12 (5 data points), and 2018 January 2 (10 data points). Measured with a precision to $0''.001$ and having estimated errors of not more than $0''.04$ according to Micheli et al. (2018), the HST positions leave, from Nakano’s gravitational solution, steady residuals of $+0''.1$ in right ascension and $+0''.1$ to $+0''.2$ in declination on November 21–22; of $+0''.4$ to $+0''.5$ in right ascension and $+0''.1$ to $+0''.2$ in declination on December 12; and of $-0''.1$ to $-0''.2$ in right ascension and $-0''.2$ in declination on January 2. On the other hand, the same HST positions leave, from Nakano’s nongravitational solution, equally consistently the residuals of $0''.0$ in both right ascension and declination on November 21–22; of $+0''.1$ in right ascension and $0''.0$ in declination on December 12; and of $0''.0$ in right ascension and $-0''.1$ in declination on January 2.

To summarize: the unsatisfactory residuals that are left by Nakano’s *gravitational* solution from the HST positions absolutely demand the presence of a nongravitational acceleration, fully confirming the conclusion by Micheli et al. and not justifying Katz’s doubts. Whereas the residuals left by Nakano’s *nongravitational* solution are much better, they are not systematic-trend free, suggesting, again in agreement with Micheli et al.’s conclusion, that the Style II nongravitational law does not provide an optimum solution either, thereby **dismissing the sublimation of water ice as the trigger capable of precipitating the orbital perturbation**, which remains unaccounted for in the outgassing model.

On the other hand, as a fair approximation, Nakano’s nongravitational solution is expected to provide a meaningful estimate for the nongravitational parameters. For the parameter of the acceleration’s radial component he found $A_1 = (+5.03 \pm 0.11) \times 10^{-4} \text{ cm s}^{-2}$, as opposed to Micheli et al.’s $(+4.92 \pm 0.16) \times 10^{-4} \text{ cm s}^{-2}$, within 1σ of each other, while the transverse component’s parameter equaled $A_2 = (-0.055 \pm 0.042) \times 10^{-4} \text{ cm s}^{-2}$, suggesting that it was essentially zero and should not have been solved for, once again in agreement with Micheli et al.’s findings. Thus, Nakano’s results offer no evidence to compromise Micheli et al.’s results.

⁹ The relevant upper limit provided by Trilling et al. (2018) for ‘Oumuamua’s *semimajor* axis, based on the object’s nondetection by the Spitzer Space Telescope, is 171 meters, compared with 260 meters derived by Seligman et al. (2019).

¹⁰ Incredibly, both the disparity noted in footnote 9 and the misquoting of Trilling et al.’s (2018) upper limit of Q_{CO} passed peer review of Seligman et al.’s (2019) paper uncorrected.

The task to compute an orbit of ‘Oumuamua was also undertaken by B. J. Gray (*Project Pluto*), whose elements and residuals (given to at least $0''.001$) from the same 200+ observations are online.¹¹ Gray was more strict with the observations than Nakano, rejecting 14 of those showing the residuals that exceeded $1''$ (but not all of them); his solution has a mean residual of $\pm 0''.278$. The nongravitational effect is expressed in terms of an “area-to-mass ratio”, which assumes an r^{-2} law. The obtained value of $10.446 \pm 0.346 \text{ cm}^2 \text{ g}^{-1}$ is equivalent to a radial acceleration of $(+4.74 \pm 0.16) \times 10^{-4} \text{ cm s}^{-2}$ at 1 AU from the Sun, within approximately 1σ of Micheli et al.’s (2018) result. The residuals from the HST observations are of interest for comparison with Nakano’s; they range from $-0''.001$ to $-0''.012$ in right ascension and from $+0''.005$ to $+0''.019$ in declination on November 21–22; from $-0''.009$ to $+0''.039$ in right ascension and from $-0''.037$ to $+0''.003$ in declination on December 12; and from $-0''.018$ to $+0''.018$ in right ascension and from $-0''.019$ to $+0''.007$ in declination on January 2. Thus, the systematic trends are now, in the worst case, at a level of $0''.01$ to $0''.02$, or about one order of magnitude smaller than Nakano’s (2018). Note that if rounded off to one decimal only, all HST residuals would be zero(!) and that Gray’s solution uses Micheli et al.’s preferred nongravitational law.

Another orbit determination effort is by Micheli’s first co-author D. Farnocchia. The results are regarded as independent because the nongravitational solution, presented on the website of the *JPL Small-Body Database Browser*,¹² employs a new sublimation law,

$$g(r) = 0.04084 \left(\frac{r}{5}\right)^{-2} \left[1 + \left(\frac{r}{5}\right)^3\right]^{-2.6}, \quad (36)$$

which should better accommodate the observations than the Style II law. All three components of the nongravitational acceleration were included in the solution, with the parameters

$$\begin{aligned} A_1 &= (+5.59 \pm 0.72) \times 10^{-4} \text{ cm s}^{-2}, \\ A_2 &= (+0.29 \pm 0.49) \times 10^{-4} \text{ cm s}^{-2}, \\ A_3 &= (+0.32 \pm 0.45) \times 10^{-4} \text{ cm s}^{-2}. \end{aligned} \quad (37)$$

Obviously, A_2 and A_3 are meaningless. The mean residual, $\pm 0''.436$, is fairly large, possibly because Farnocchia included 15 more observations in the solution than Gray, some of them presumably leaving larger residuals. However, since the individual residuals are unavailable on the website, this cannot be stated with certainty. The larger error of A_1 could be an effect of the correlations between the nongravitational parameters and the same might be true about the value of A_1 . Nonetheless, even so the deviation of A_1 from $4.92 \times 10^{-4} \text{ cm s}^{-2}$ is less than 15 percent. I conclude that **Micheli et al.’s results are confirmed by all three presented orbital analyses; comparison of the HST residuals from Nakano’s and Gray’s solutions shows that the inverse square law is superior to the Style II law, in line with independent evidence implying that the sublimation of water ice is not triggering the nongravitational acceleration.**

In the context of ‘Oumuamua’s extremely low bulk density inferred from the considerations in the previous sections, it is noted that Kataoka et al. (2013) provide a pathway for long-term growth of a fluffy aggregate of submicron-sized dust grains into a planetesimal in a protoplanetary disk (see also Kataoka 2017). According to these authors, the initial assembly of grains, each 10^{-15} g in mass and of material density, reaches eventually a terminal mass of 10^{18} g and a diameter of 10 km. The earliest stage of the evolution is dominated by low-velocity collisional coagulation, in which the bulk density of the dust aggregate of steadily augmenting dimensions keeps dropping as an inverse square root of mass (i.e., with a mass fractal dimension of 2). Growth of the aggregate gradually invokes collisional compression, whose effect however is not enough to reverse the trend toward increasing porosity until the bulk density drops to as low as $0.00002 \text{ g cm}^{-3}$, at which time the aggregate is $\sim 10^{-5} \text{ g}$ in mass and nearly 1 cm across. The aggregate’s slow compaction, leading to an increase in the bulk density by about one order of magnitude by the time the mass is some 100 g and diameter 1 m, is largely a product of quasi-static compression by ambient gas in the protoplanetary disk. However, in the mass range from 10 kg to a million tons (spanning eight orders of magnitude!) the bulk density is remarkably flat, staying between 0.0002 and 0.0004 g cm^{-3} at all times until self-gravity sets in, when the object is hundreds of meters across and getting rapidly denser from that point on.

Assuming that ‘Oumuamua was the largest inactive fragment of an interstellar comet that was an embryo planetesimal in a stage of evolution that had preceded the self-gravity compression stage, the former’s mass should be a non-negligible fraction of the latter’s. For the parent’s assumed diameter of $\sim 120 \text{ m}$ and bulk density of $\sim 0.0003 \text{ g cm}^{-3}$ in this stage of evolution, its mass was equal to a few times 10^8 g in Kataoka’s (2017) plot, so that the mass of 10^7 g , proposed for ‘Oumuamua’s fluffy model (Sekanina 2019a), fits the notion of the parent’s “skeleton” residuum, amounting to several percent of the mass upon arrival at the inner Solar System in early 2017, a plausible outcome of the parent’s putative disintegration near perihelion.

8. CONCLUSIONS

At the time of Micheli et al.’s (2018) paper on the nongravitational effects in ‘Oumuamua’s orbital motion, there were only two warning signs that made activity highly questionable as the acceleration’s trigger: one was the object’s star-like appearance, which indicated an extremely low level of dust production (Meech et al. 2017); the other was the strict constraint on the production of CN, C₂, and C₃ (Ye et al. 2017). For some reason, neither argument turned out to be strong enough to deter the proponents. A third warning sign, the sublimation law, was brought up by Micheli et al. themselves, but it related only to the production of water and it seems that its significance was downplayed. The most damaging finding to the outgassing hypothesis was the very tight limit of the abundances of CO₂ and CO derived by Trilling et al. (2018), not available until months later. With both carbon-bearing volatiles eliminated as the prime mover of activity, water ice remained the only hope of the outgassing hypothesis.

¹¹ See <https://projectpluto.com/temp/2017u1-a.htm>.

¹² See Orbit 16 on <https://ssd.jpl.nasa.gov/sbdb.cgi>.

This paper elaborates on the grave difficulties one confronts in an attempt to identify the sublimation of water ice with ‘Oumuamua’s presumed activity and with the trigger of the detected nongravitational acceleration:

(a) the variation with heliocentric distance is incompatible with the law that fits the orbital data;

(b) the acceleration exceeds the outgassing-driven accelerations of practically all comets, while the star-like appearance of ‘Oumuamua is in sharp contrast with the considerable diffuseness of C/1998 P1 and other comets with sizable (yet presumably outgassing-induced) nongravitational effects; and

(c) the absence of detectable activity is shown in Sections 5–6 to imply that the sublimation of water ice proceeded, if it did at all, from only a very small fraction of the surface and that the bulk density would have to be extremely low, below 0.001 g cm^{-3} ; the porosity and morphology would then readily fit the scenario in which ‘Oumuamua was described as an inactive fragment of a dwarf interstellar comet that had disintegrated near perihelion weeks before discovery (Sekanina 2019a). This hypothesis is also consistent with the parent comet having been an embryo planetesimal in the coagulation growth pathway of fluffy dust aggregates constructed by Kataoka et al. (2013) and Kataoka (2017). The nongravitational acceleration of ‘Oumuamua was then driven by solar radiation pressure, in which case there indeed should be no need for even a trace of activity; not to mention that the difficulties under (a) and (b) disappear by default.

While I see no avenue for outgassing in general, and the sublimation of water ice in particular, to perform as a trigger for ‘Oumuamua’s nongravitational acceleration, it should be acknowledged that it is the high-quality imaging, image processing, astrometric work, as well as the superb orbital analysis available that made it possible to constrain the model to this extent.

This research was carried out at the Jet Propulsion Laboratory, California Institute of Technology, under contract with the National Aeronautics and Space Administration.

REFERENCES

- A’Hearn, M. F., Millis, R. L., Schleicher, D. G., et al. 1995, *Icarus*, 118, 223
- Bair, A. N., Schleicher, D. G., & Knight, M. M. 2018, *AJ*, 156, 159
- Bodewitz, D., Villanueva, G. L., Mumma, M. J., et al. 2011, *AJ*, 141, 12
- Do, A., Tucker, M. A., & Tonry, J. 2018, *ApJ*, 855, L10
- Drahus, M., Guzik, P., Waniak, W., et al. 2018, *Nature Astron.*, 2, 407
- Farnham, T. L., Schleicher, D. G., Woodney, L. M., et al. 2001, *Science*, 292, 1348
- Hale, A. 2000, *Int. Comet Quart.*, 22, 44
- Kataoka, A. 2017, in *Formation, Evolution, and Dynamics of Young Solar Systems*, ed. M. Pessah & O. Gressel, *Astrophysics and Space Science Library*, 445 (Cham, Switzerland: Springer), 143
- Kataoka, A., Tanaka, H., Okuzumi, S., & Wada, K. 2013, *A&A*, 557, L4
- Katz, J. I. 2019, *Astrophys. Space Sci.*, 364, 51
- Knight, M. M., & Schleicher, D. G. 2015, *AJ*, 149, 19
- Lupu, R. E., Feldman, P. D., & Weaver, H. A. 2007, *ApJ*, 670, 1473
- Marsden, B. G., & Williams, G. V. 2008, *Catalogue of Cometary Orbits 2008*, 17th ed. (Cambridge, MA: IAU Minor Planet Center/Central Bureau for Astronomical Telegrams), 195pp
- Marsden, B. G., Sekanina, Z., & Yeomans, D. K. 1973, *AJ*, 78, 211
- Meech, K. J., Weryk, R., Micheli, M., et al. 2017, *Nature*, 552, 378
- Micheli, M., Farnocchia, D., Meech, K. J., et al. 2018, *Nature*, 559, 223
- Mumma, M. J., Dello Russo, N., DiSanti, M. A., et al. 2001, *Science*, 292, 1334
- Nakano, S. 2018, *NK* 3691
- Ootsubo, T., Usui, F., Kawakita, H., et al. 2010, *ApJ*, 717, L66
- Ootsubo, T., Kawakita, H., Hamada, S., et al. 2012, *ApJ*, 752, 15
- Park, R. S., Pisano, D. J., Lazio, T. J. W., et al. 2018, *AJ*, 155, 185
- Probstein, R. F. 1969, in *Problems of Hydrodynamics and Continuum Mechanics*, ed. F. Bisshopp & L. I. Sedov (Philadelphia: Soc. Ind. Appl. Math.), 568
- Reach, W. T., Kelley, M. S., & Vaubaillon, J. 2013, *Icarus*, 226, 777
- Sekanina, Z. 1982, in *Comets*, ed. L. L. Wilkening (Tucson, AZ: University of Arizona), 251
- Sekanina, Z. 1993, *AJ*, 105, 702
- Sekanina, Z. 2019a, eprint arXiv:1901.08704
- Sekanina, Z. 2019b, eprint arXiv:1903.06300
- Sekanina, Z., & Kracht, R. 2015, *ApJ*, 801, 135
- Seligman, D., Laughlin, G., & Batygin, K. 2019, *ApJ*, 876, L26
- Trilling, D. E., Mommert, M., Hora, J. L., et al. 2018, *AJ*, 156, 261
- Yabushita, S. 1996, *MNRAS*, 283, 347
- Ye, Q.-Z., Zhang, Q., Kelley, M. S. P., & Brown, P. G. 2017, *ApJ*, 851, L5